Exchange stiffness constant determination using multiple-mode FMR perpendicular standing spin waves

DOI:
10.1063/5.0135024

Document Version
Accepted author manuscript

Exchange Stiffness Constant Determination using Multiple-Mode FMR Perpendicular Standing Spin Waves

H. J. Waring[1], Y. Li[1], N.A.B. Johansson[1], C. Moutafis[1], I. J. Vera-Marun[2], T. Thomson*[1]

[1] Nano-Engineering and Spintronic Technologies (NEST), Department of Computer Science, University of Manchester, Manchester, M13 9PL, UK.

[2] Department of Physics and Astronomy, University of Manchester, Manchester, M13 9PL, UK.

ABSTRACT

The exchange stiffness constant is recognised as one of the fundamental properties of magnetic materials, though its accurate experimental determination remains a particular challenge. In thin films resonance measurements exploiting Perpendicular Standing Spin Waves (PSSWs) are increasingly used to extract this parameter, typically through a determination of the first order PSSW mode. Here we present a systematic study of multiple PSSW modes in NiFe films, where both sample thickness and cap layer material are varied. The results show that a simple analysis based on the Kittel rigid pinning model yields an exchange stiffness constant that varies with thickness, mode number and capping layer material. This finding is clearly inconsistent with the physical expectation that the exchange stiffness constant of a material is single valued for a particular set of thermodynamic conditions. Using a more general exchange boundary condition we show, through a comprehensive set of micromagnetic simulations, that a dynamic pinning mechanism originally proposed by Wigen is able to reproduce the experimental results using a single value of A_{ex}. Our findings support the utility of short wavelength, higher order PSSWs to determine the A_{ex} of thin films and show that the value of A_{ex} obtained has a weak dependency on the material immediately adjacent to the magnetic layer.

* Corresponding author: thomas.thomson@manchester.ac.uk

I. INTRODUCTION

The exchange stiffness constant (A_{ex}) together with the saturation magnetisation (M_S), Curie temperature (T_c) and the anisotropy (K) are the four fundamental properties of magnetically ordered materials [1]. These parameters determine the nature of the magnetic ordering and thus an accurate characterisation is crucial in advancing fundamental understanding and technological application of magnetic thin film materials. Whilst it is possible to accurately determine M_S, T_C and K directly from magnetometry measurements provided suitable temperature ranges and magnetic fields can be applied, A_{ex} cannot be as readily ascertained. The increasing interest in magnetisation dynamics is driven by the fields of spintronics and magnonics where next generation device functionality will be reliant on high frequency magnetic processes[2]–[6]. Thus, an enhanced understanding would impact technologies such as magnetic memories [3], [6]–[9], Spin-Torque Nano Oscillators [5], [6], [9], [10], signal processing[6] and sensors[8], [9], [11], [12]. Furthermore, as the exchange stiffness constant is required as an input parameter for atomistic and micromagnetic modelling, an accurate determination of this value in real materials is vital in ensuring the validity of simulations of magnetic processes, a growing and important aspect in magnetics research [13], [14].

There are several experimental approaches that are commonly used to obtain the exchange stiffness constant using Bloch's $T^{3/2}$ Law [15], [16]. This technique involves determining the variation of M_S at low temperatures due to a gradual magnetisation twist generated by low-energy, long-wavelength spin waves (thermal magnons). This approach assumes that the reduction in magnetisation is due only to thermal magnons and hence is typically limited temperatures that are a fraction of the Curie temperature[16]. To address this, there has been an increasing interest in the study of magnetization dynamics to determine A_{ex} at room temperature. Two measurement techniques are used to determine A_{ex} in thin film systems, namely ferromagnetic resonance (FMR) spectroscopy [15]–[18] and Brillouin light scattering (BLS) [19]–[22]. BLS is a well-established technique in the study of magnetisation dynamics involving the measurement of the inelastic scattering of photons from magnetic materials due to the generation of spin waves [23]. It offers a large frequency range spanning 1 GHz to 500 GHz, a corresponding frequency resolution of 50 MHz and a very high sensitivity [24]. Neutron scattering is also an important technique to determine A_{ex} [25] though is outside the capabilities of most laboratories.

Here we focus on an FMR technique which relies on the observation of higher order spin wave resonances dominated by the exchange stiffness constant, which manifest in the direction perpendicular to the plane of the film due to the constraints of film thickness, known as Perpendicular Standing Spin Waves (PSSWs) [26]. PSSW resonances were originally predicted by Kittel [27] with experimental detection demonstrated by Seavey et. al. [28]. A schematic of the form of PSSWs for the two extreme cases of (a) no pinning (sometimes referred to as natural pinning) and rigid pinning (sometimes referred to as perfect pinning) are shown in Fig. 1. In the case of symmetric boundary conditions, only odd order modes will be excited while even modes can be excited for asymmetric boundary conditions where there are different pinning conditions on upper and lower interfaces but these are frequently weak as the asymmetry is typically rather small.

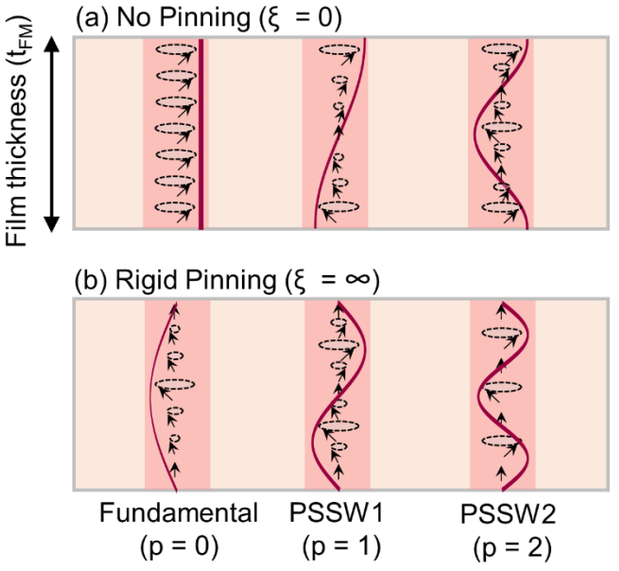

FIG. 1. Schematic of the spin configuration of Perpendicular Standing Spin Waves (PSSWs) of different mode number p across film thickness (t_{FM}). The arrows represent the precessing spins, with these profiles assuming that the pinning parameter (ξ) is, a) $\xi = 0$ for the unpinned case and, b) $\xi \to \infty$ for the case of rigid pinning of the surface spins (Kittel model).

Measurements and analysis of PSSWs depend crucially on the nature of the interface between the ferromagnetic thin film and the adjacent medium. This interface is typically characterised by a pinning parameter [29] of the form:

$$\xi = \frac{2K_s}{qM_s^2} \tag{1}$$

where K_s is surface anisotropy and $q = \nabla^2 \boldsymbol{M}$ is the non-uniform part of the effective exchange field which characterises the degree of fastening of the magnetic moments at the boundary[29]. The limiting cases of no pinning or free magnetic moments $(\xi = 0)$ was first employed by Ament and Rado [30] and perfect rigid pinning ($\xi \to \infty$) was proposed by Kittel [27] with the general case studied by Rado and Weertman[31].

The special case of rigid surface pinning [27], [32] provides the simplest method for the analysis of PSSWs where the frequency for a thin film dominated by shape anisotropy is related to A_{ex} by

$$f_{PSSW} = \frac{\gamma}{2\pi}\left(H_{ext} - 4\pi M_S + \frac{2A_{ex}}{M_S}\frac{p^2\pi^2}{t_{FM}^2}\right), \tag{2}$$

where γ is the gyromagnetic ratio, H_{ext} is the externally applied magnetic field, M_S is the saturation magnetisation, p is the mode number above the fundamental mode and t_{FM} is thickness of the ferromagnetic layer [23,26]. However there are reports that the A_{ex} determined from different PSSW modes analyzed using Eq. 2 can vary [32]–[35]. Given that higher order modes have comparatively low intensities, typically only the first excited PSSW mode (p = 1) is utilised [36]–[38].

Hence, a more detailed understanding of the variation of the A_{ex} determined from different order PSSWs is required.

In the rigid pinning Kittel model the wavevector is described by

$$k \quad = \frac{p\,\pi}{t}, \tag{3}$$

where *t* is the film thickness. It follows that the mode number *p* must have integer values of 1 or greater in this analysis and that the fundamental mode has *p* = 1 rather than *p* = 0. Note that a detailed analysis of pinning has been reported by Puszkarski [39] and by Maksymowicz [40]. In their work the concept of a generalised wavevector is employed, which enables us to underline the fundamental link between the pinning conditions and the wavevector for standing spin wave modes. To avoid confusion, we label the mode number of this generalised wavevector as $p_k$and maintain the nomenclature of fig. 1 to describe our data and results. Using this generalised approach,

$$k_p = (p_k + \delta)\frac{\pi}{t} = \frac{2\,\pi}{\lambda_p}, \tag{4}$$

where $\lambda_p$the wavelength of the excitation and the parameter δ, whose value can vary between $0 < \delta < 1$, gives some measure of the degree of pinning present (δ at each interface for symmetric pinning). This form of the wavevector allows intermediate cases of pinning to be parametrised, with $\delta = 0$ corresponding to no pinning, and $\delta = 1$ to rigid pinning. Furthermore, this form can also allow the case for asymmetric pinning, with two distinct values at each interface, δ_1 and δ_2, by considering $\delta = (\delta_1 + \delta_2)/2$. This generalised approach yields a perpendicular standing wave frequency, after modifying Eq. (2), which is described by:

$$f_{PSSW} = \frac{\gamma}{2\pi}\left(H_{ext} - 4\pi M_S \; + \frac{2A_{ex}}{M_S}k_p^2\right). \tag{5}$$

In this work, we first analyse our PSSW data measured for a series of NiFe thin films with different thickness and capping layer materials (uncapped, Pt and Ta) using the two analytical models described by Eqs (2) and (5). We then present detailed micromagnetic simulations based on the dynamic pinning (DP) model where the magnetic properties of the interfaces are modified relative to the "bulk" of the thin film.

We show that the rigid pinning model when applied to the first excited PSSW mode does not provide a consistent value of the exchange stiffness constant. On the other hand, the second excited mode yields a more consistent result. The generalised wavevector model can provide a consistent value of exchange stiffness constant, for both PSSWs, by suitable adjustment of the pinning parameter δ, but that values of A_{ex} are lower than generally expected from the literature. Using micromagnetic simulations, we are able to obtain values of the exchange stiffness constant that are both consistent across the modes and films thicknesses and in excellent agreement with the literature.

A knowledge of the effect of different ferromagnetic/non-magnetic interfaces on the value of A_{ex} obtained from PSSWs provides further insight into the characterisation of these materials and their potential use in spintronic applications[6], [41], [42].

II. SAMPLE PREPARATION AND STRUCTURAL CHARACTERISATION

A series of samples was produced by magnetron sputtering onto Si/SiO_2 substrates (see Appendix A). The multilayer structure was $Ni_{0.8}Fe_{0.2}(t_{NiFe})/X$ where t_{NiFe} is NiFe layer thickness, varied between t_{NiFe} = 23 nm and t_{NiFe} = 102 nm, and X is the capping layer material (uncapped, Pt and Ta). NiFe was chosen as the ferromagnetic material as this has been widely studied and serves as a useful model system [43]–[46]. In order to unambiguously identify the effect of the capping layer, a seedlayer was not used in the stack structure due to the possibility this may introduce a variation in pinning boundary conditions at this interface. The layer structure of the multilayers was determined using X-Ray Reflectivity (XRR) where the data were fitted to a Fresnel model using the GenX software package [47]. It was found that in the uncapped case a self-passivating Fe_2O_3/NiO bilayer formed consistent with literature expectations[45] whilst the Ta capping layer case formed a self-passivating Ta_2O_5 layer (for additional information regarding the XRR measurements of the samples see Appendix B1 and Fig. 7). The roughness of the NiFe layer at the interface was determined from the fits to the XRR data and was similar for all samples with an average value of 1.7 ± 0.4 nm.

III. Magnetic Characterization and Perpendicular Standing Spin Waves

The static magnetic properties of the samples were determined using Vibrating Sample Magnetometry (VSM) (details in appendix B2). Table I presents the averaged magnetic parameters of the films for each capping layer case as extracted from VSM measurements, demonstrating that these values are consistent irrespective of capping layer material.

Table I: Average magnetic properties of the samples in each capping layer case over the range of studied film thickness as measured by VSM and VNA-FMR. The values and uncertainties are obtained from averaging all the films measured for each capping layer series.

Capping Layer	VSM: M_S (emu/cm^3)	g	FMR: M_{Eff} (emu/cm^3)
Uncapped	720 ± 30	2.07 ± 0.03	690 ± 30
Pt Capped	700 ± 50	2.06 ± 0.04	700 ± 30
Ta Capped	720 ± 50	2.07 ±0.01	730 ± 10

Magnetisation dynamics were measured using a broadband Vector Network Analyzer-Ferromagnetic Resonance Spectrometer (VNA-FMR (details in Appendix B3). The resonant absorption was obtained from the VNA S_{12} absorption parameter, which was then used to determine the resonant frequency. The values of the effective magnetisation and g-factor extracted from fitting the Kittel FMR equation [48] to the fundamental mode are also shown in Table I.

The PSSW spin-wave spectra obtained by applying the external magnetic field Out-Of-Plane (OOP) and example data for the case of a Ta capped NiFe layer with t_{NiFe}= 86 nm are presented in Fig. 2, where a fundamental resonance (FMR) mode and higher order PSSWs are observed. The data were analysed in the region where the strength of the applied magnetic field ensured that the samples were fully saturated (> 11 kOe). These data show that the peak amplitudes of the PSSWs reduce

significantly with mode number, as expected [26] which can lead to greater uncertainty in the parameters extracted from the measurements. The detected PSSWs were designated PSSW1 for p = 1 (first excited mode) and PSSW2 for p = 2 (second excited mode) respectively. The formation of PSSW resonances at an external field strength greater than ~10 kOe is consistent with the field required to saturate the NiFe film in the OOP direction in static measurements (refer to Appendix B2 and Fig. 8).

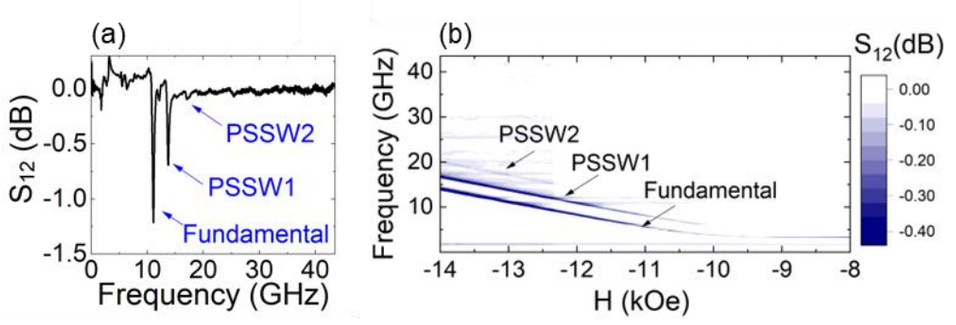

FIG. 2: The spin-wave spectra of a Ta capped NiFe layer with thickness t_{NiFe} = 86 nm. a) S_{12} spectra at an applied field of 13 kOe. b) A 2D map of the resonant spectrum as a function of applied field and frequency.

To demonstrate how different pinning assumptions affect the results obtained, we first analyse the experimental data in terms of $A_{ex,app}$ before demonstrating through micromagnetic simulation that the dynamic pinning model proposed by Wigen [49] is able to describe the measured data with a single value of A_{ex}. The exchange stiffness constant was extracted from the PSSW modes exhibited by each NiFe thin film using Eq. (2). Figure 3 (a-c) show the extracted exchange stiffness constant for all capping layer cases as a function of t_{NiFe} and p. Strikingly, the data demonstrate that a single A_{ex} is unable to describe the experimentally measured resonances using the rigid pinning model given by Eq. (2). This finding that is clearly inconsistent with the normal assumption that the exchange stiffness constant has a single value which for NiFe close to 1x10^{-6} erg/cm[15]. There are a very limited number of reports on the variation of A_{ex} as determined from PSSWs of different mode number in the literature [32]–[34]. This demonstrates that the rigid pinning Kittel model does not fully describe the complexities of PSSWs, leading to the extraction of an apparent exchange stiffness constant ($A_{ex,app}$) dependent on the PSSW mode rather than the true exchange stiffness constant of the ferromagnetic material.

The two detectable PSSW modes show different behaviour with increasing t_{NiFe} and p. In the case of PSSW1, it is observed that in all capping layer cases there are two regimes for the variation of $A_{ex,app}$ as t_{NiFe} increases. At layer thicknesses lower than ~55 nm it can be observed that $A_{ex,app}$ is approximately constant. However, at thicknesses greater than 55 nm, $A_{ex,app}$ shows a monotonic increase. Similar variations have been reported by Belmeguenai et al. [38], although this was attributed to a lack of precision in their work, and by Samantaray [33].

In the case of PSSW2, which was only reliably detected for t_{NiFe}> 50 nm, $A_{ex,app}$ is less than that determined from the corresponding PSSW1 mode. Furthermore, the $A_{ex,app}$ extracted from PSSW2 shows no significant dependence on t_{NiFe} apart from in a singular case at the highest t_{NiFe}

examined in the Pt capped sample series. It is notable that the $A_{ex,app}$ extracted from PSSW2 is similar to that extracted from the PSSW1 modes of films with t_{NiFe}< 55 nm. This suggests that as film thickness reduces the value of $A_{ex,app}$ extracted from PSSW1 reaches an asymptotic value, potentially providing a value for the exchange stiffness constant in films too thin to support detectable PSSWs.

These data demonstrate that the capping layer material does have an impact upon the $A_{ex,app}$ determined for each sample. The data show that Pt capped samples are able to support the higher order PSSW2 mode at a lower t_{NiFe} than seen in the uncapped or Ta capped cases. Additionally, for the cases of the Pt and Ta capped layers, the $A_{ex,app}$ determined using PSSW1 increases linearly with t_{NiFe} with greater increases found for the Pt capped films. In general, higher $A_{ex,app}$ values are obtained from both the PSSW1 and PSSW2 modes in the case of Pt capped layers with uncapped films showing the lowest values of $A_{ex,app}$.

The variation of $A_{ex,app}$ with PSSW wavelength (λ_{PSSW}) has also been explored. The wavelength of the spin waves was determined using Eqs. (4) and (5). Fig.3(d-f) demonstrates that longer wavelength spin excitations lead to the extraction of a higher $A_{ex,app}$, with a similar trend seen in all capping layer cases. It can be seen that the third term on the RHS of Eq. (5) (containing A_{ex}) represents the exchange contribution to the PSSW mode frequency and that this becomes more dominant for higher order and shorter wavelength PSSWs. Therefore, the greater consistency of $A_{ex,app}$ in the cases of PSSW1 <55nm or PSSW2 can be readily explained as for these spin waves the exchange term can dominate and partially screen unaccounted for effects in Eq. 1, such as dynamic pinning. This is consistent with the proposition that the value of $A_{ex,app}$ tends to an asymptotic value and hence may provide a way to estimate the exchange stiffness constant of thinner films where PSSWs are not measurable.

Next, we explore the general case of partial pinning. For this, we use Eqs. (4) and (5) with the condition of a finite value of the parameter δ. The latter is adjusted to an appropriate value, for each different capping layer, which provides a single-valued exchange stiffness constant for both PSSW1 and PSSW2 modes. As seen in Fig. 3, the result averaged across all thicknesses leads to an extracted exchange stiffness constant for NiFe of 0.9 x 10^{-6} erg/cm for uncapped and Ta capped, and 0.7 x 10^{-6} erg/cm for Pt capped. This method offers a more robust model, using the same integer mode numbers as for the idealised no pinning and rigid pinning cases. The boundary condition with partial pinning can be seen as a physical interpretation of the dynamic pinning model proposed by Wigen [49] mentioned above, which we will explore below via numerical modelling.

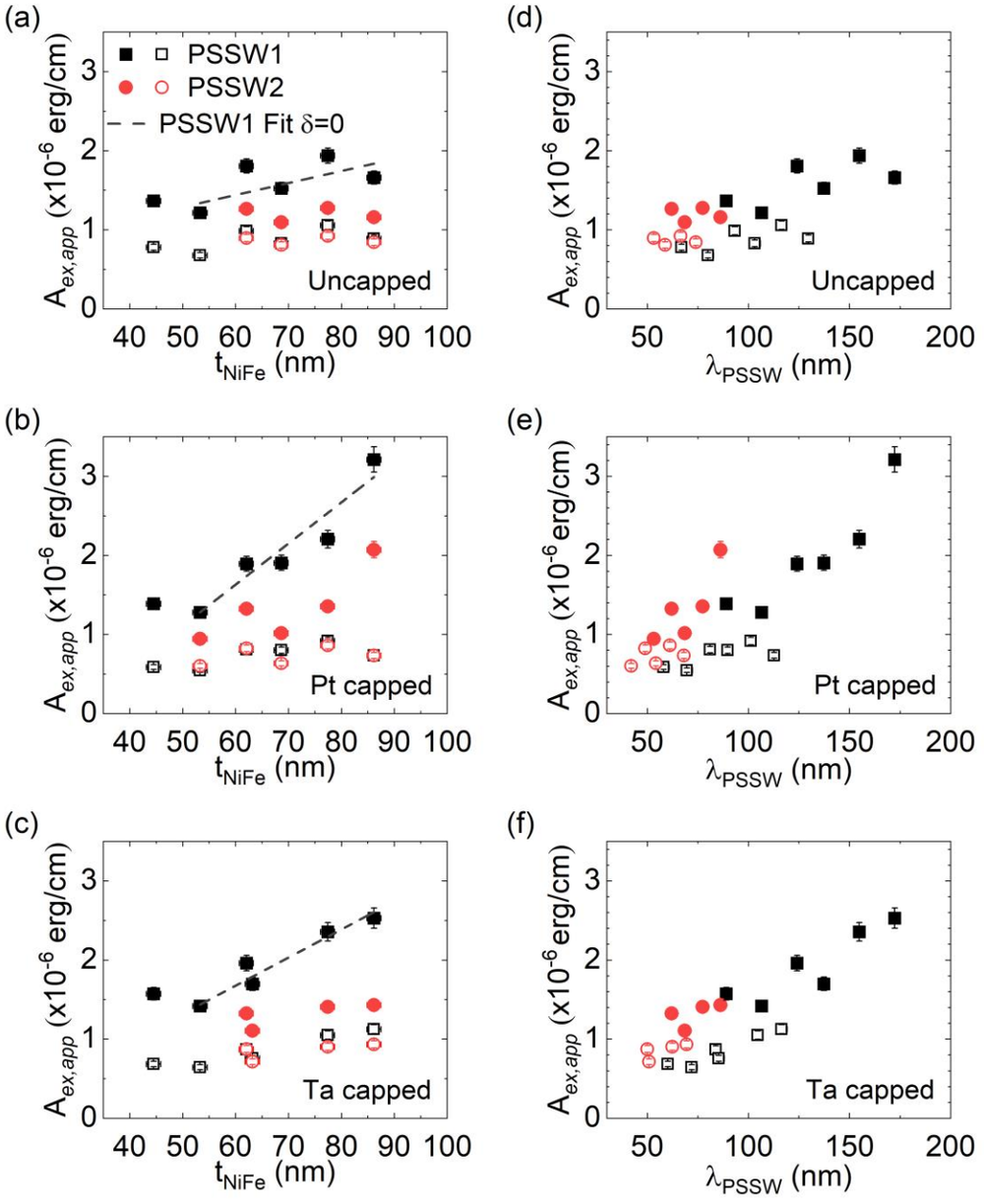

FIG. 3: The variation of $A_{ex,app}$ determined using Eq. (5) in each capping layer case from a study of the PSSWs with (a-c) t_{NiFe} and p for each capping layer case and (d-f) λ_{pssw} for each capping layer case. The dashed line is a linear fit to the PSSW1 data which shows an increase of $A_{ex,app}$ with film thickness. Closed symbols correspond to the case of 'no pinning' with δ = 0. Open symbols correspond to the generalised case of dynamic pinning, with δ = 0.33, 0.47, 0.52 for uncapped, Pt capped, and Ta capped, respectively. The error bars are within the symbols for some data.

IV. Simulation Using a Single Exchange Stiffness Constant

Numerical modelling has been performed to reconcile the physically required concept of a single valued exchange stiffness constant with the experimentally measured resonances. The simulations were done using the micromagnetic modelling package Mumax[3] which is a finite-difference GPU-accelerated simulation program[50]. The magnetic parameters input to the model were chosen to be consistent with NiFe in order to allow direct comparison of the simulation results with the experimental measurement. Specifically, the damping parameter was set to α = 0.001, the exchange stiffness constant varied between A_{ex} = 1x10^{-6} erg/cm and A_{ex} = 1.6x10^{-6} erg/cm and M_S was set as experimentally determined from the FMR data for each sample. In order to minimise the demagnetisation effects from the physical edge, periodic boundary conditions were applied in-plane. The overall system is discretised into 2 nm x 2 nm x 1 nm cuboid cells and the dimension in the *xy*-plane set to 128 nm x 128 nm. The ringdown method was used to obtain the free induction decay of the magnetisation which was then Fourier transformed to obtain the ferromagnetic resonance frequency (see Appendix C for more details regarding the simulation procedure).

The results presented in Fig. 3 demonstrate that an analysis based on the assumption of rigid pinning (Kittel model) does not allow the PSSW resonant frequencies to be reproduced using a single A_{ex}. To resolve this inconsistency, we show that a dynamic pinning mechanism originally proposed by Wigen [49] is able to reproduce the experimental results using a single value of A_{ex}. In this model, the surface of the thin film consists of a few atomic layers where the internal field differs by a small amount from that of the bulk of the film. Dynamic pinning describes the case that whilst the spins close to the surface are not rigidly pinned and can precess but with a different external field or frequency for resonance compared to that of the bulk of the film. This leads to a pinning which only becomes apparent during dynamic measurements of the film. Such an effect can arise from a number of mechanisms including a change in the anisotropy field perpendicular to the film, a different state of strain for these surface layers due to the magnetoelastic effect, or a difference in the magnetisation of the surface layer resulting in an altered demagnetisation field[49], [51]. Dynamic pinning was introduced to the structure by modelling the thin film as two regions of magnetisation satisfying the following conditions:

i) The bulk layer possessed a magnetisation set to that extracted as M_S from fundamental FMR mode of each film. The thickness of this layer was set to the measured t_{NiFe}.

ii) The presence of a few atomic layers at the interface between NiFe and capping layer material with a reduced magnetisation (M_S^R) and thickness (t^R) . The expectation of DP model is that the difference in layer magnetisation is small.

Thus, we extend the pinning parameter introduced by Rado and Weertman[30] to explicitly explore the nature of dynamic pinning. The sensitivity of the extracted A_{ex} to the magnetisation of the near-interface region and its thickness was then determined by performing a series of simulations that varied these parameters so as to compare the modelled resonances with the experimental measurements. For this step a Pt capped NiFe film with $t_{NiFe} = 55$ nm was taken as an example with the input A_{ex} varied between the literature value of the exchange stiffness constant of NiFe A_{ex} = 1x10^{-6} erg/cm [15] and A_{ex} = 1.6x10^{-6} erg/cm, M_S^R was varied between 200 emu/cm^3 and 600 emu/cm^3 and t^R between 1 nm and 5 nm[15] [15] [15]. The optimal A_{ex} for each simulated reduced

magnetisation layer case was found by comparing the experimentally measured resonant frequency of each PSSW mode to a linear fit of the simulated resonant frequency and A_{ex} input to the simulation. The results of this study are presented in Fig. 4. We note that the choice of reduced layer parameters impacts the A_{ex} extracted from PSSW1 to a slightly greater extent than for PSSW2. However, these results show that the value of A_{ex} obtained does not have a strong dependency on the reduced magnetisation layer thickness. Above 2 nm the thickness of the reduced magnetisation layer is essentially unimportant but there is some dependence, particularly for PSSW1 below approximately 1.5 nm. We note that the simulation cell thickness dimension is 1 nm and that atomistic simulations [52] would be required to further refine the estimate of the critical layer thickness for dynamic pinning. The value of the magnetisation does have some effect on A_{ex} principally when it is within 200 emu/cm^3 of the "bulk" layer. However, even in this regime the difference in A_{ex} is only ~0.1 erg/cm. These results demonstrate the robustness of this approach in determining A_{ex} whilst showing insensitivity to details of interface. Based on these results, the Ta and Pt capped samples were simulated with a dynamic pinning generated by a reduced layer parameters $M_S^R \leq 500$ emu/cm^3 and $t^R = 5$ nm. In the case of the uncapped NiFe films, the approach of modelling antiferromagnets as detailed by De Clerq et al. was followed [53]. Specifically, the reduced layer was initialised with a M_S value equal to that of the bulk layer with an antiferromagnetic coupling $A_{ex} < 0$ input (see Appendix C and ref.[53] for more details). The model was also tested by considering a system with reduced magnetisation layers on both the substrate and cap side of the bulk layer. However, this approach was unable to reproduce the experimentally measured resonances for any of the samples.

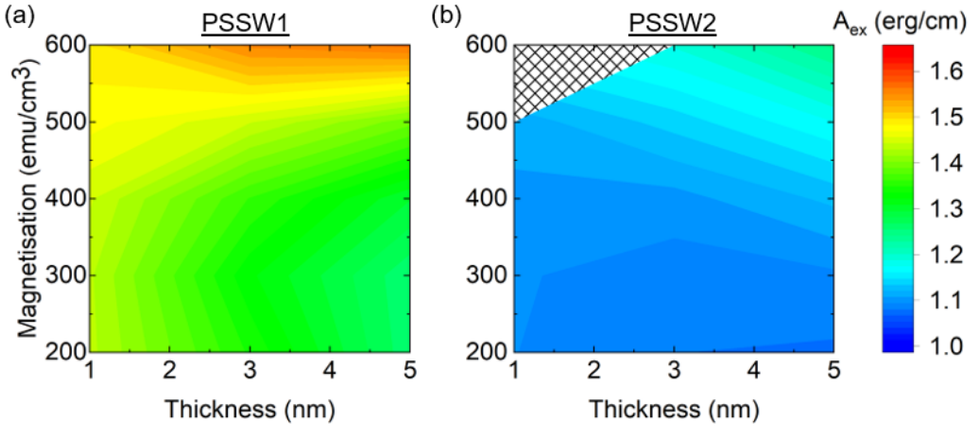

FIG. 4: The sensitivity of the extracted A_{ex} for a Pt capped NiFe film with $t_{NiFe} = 55$ nm from comparison of simulation and experiment using a) PSSW1 and b) PSSW2. The hatched region in b) shows the conditions where a PSSW could not be observed in the simulation.

The experimentally measured and resonant frequencies simulated using A_{ex} = 1 x 10^{-6}, 1.3 x 10^{-6} and 1.6 x 10^{-6} erg/cm for all observed PSSW modes are presented in Fig. 5. In all capping layer cases the resonant modes are well described by the simulation, which provides good evidence that the dominant mechanism is dynamic pinning rather than the commonly used rigid surface pinning at the interface. The simulations also model the formation of higher order PSSW modes with the modelled resonant frequency of PSSW3 (p = 3) shown in Fig. 5. The lack of these modes in the experimentally obtained spectra is due to the peak amplitude of these higher order PSSW resonance being below the detection limits of the VNA-FMR used in measurement.

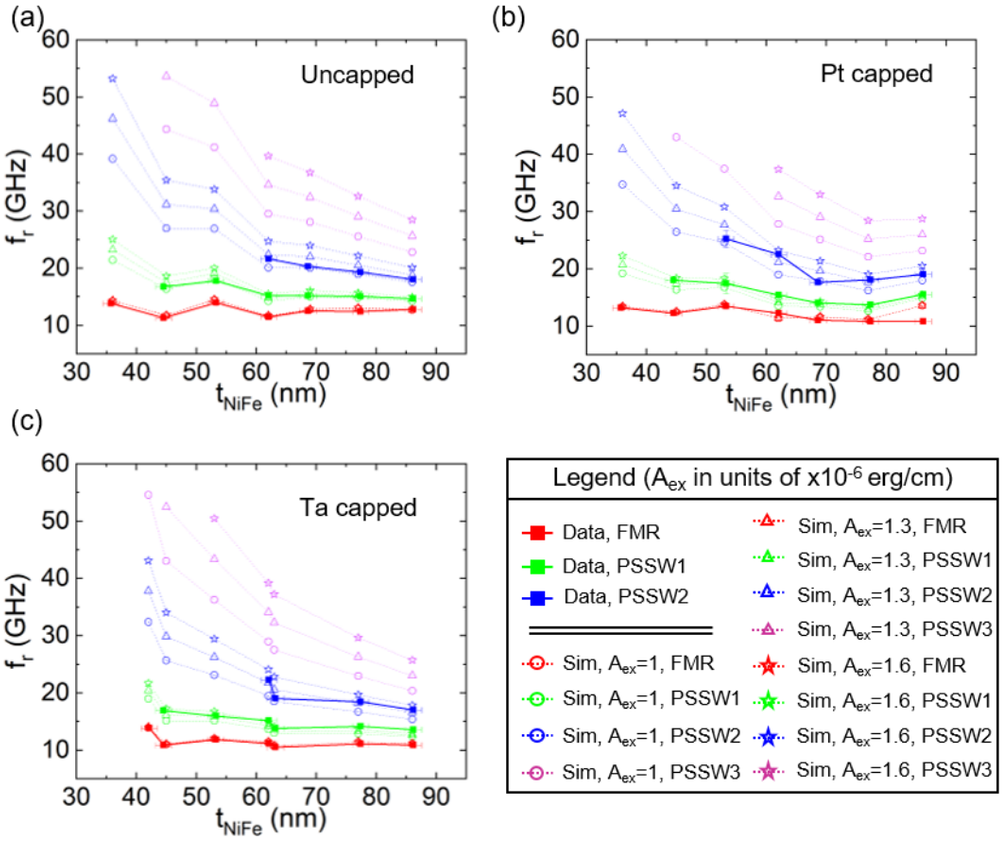

FIG. 5: Measured and simulated resonant frequencies of the spin-wave spectra exhibited for different thickness of NiFe film (t_{NiFe}). The simulations were done with three fixed values of A_{ex} (1.0 x 10^{-6}, 1.3 x 10^{-6} and 1.6 x 10^{-6} erg/cm) chosen to allow an accurate value of A_{ex} to be determined by interpolation, a) for the uncapped film, b) for the Pt capped film and c) for the Ta capped film. The lines between data points are given as a guide to the eye. The legend is common to all three (a, b and c) data panels and FMR refers to the fundamental mode.

The optimal $A_{ex}$for each capping layer case are presented in Table II, where the A_{ex} extracted from comparing the modelling and the measured PSSWs is presented.

Table II: The optimal exchange stiffness constant for the sample series in each capping layer case, as extracted from comparison between experimental measurement and simulation.

	A_{ex} (x10^{-6} erg/cm)			
Capping Layer	**PSSW1 (t_{NiFe} <55 nm)**	**PSSW1**	**PSSW2**	**All modes**
Uncapped	1.0±0.2	1.2±0.2	1.1±0.1	1.1 ±0.2
Pt Capped	1.4±0.2	1.6±0.3	1.2±0.2	1.4±0.2
Ta Capped	1.4±0.1	1.7±0.3	1.3±0.2	1.5±0.2

The data in Table II demonstrate that short wavelength PSSWs provide a more consistent value of A_{ex}, which is also close to the literature values, and thus is consistent with the conclusion drawn

from data presented in Fig. 3(d-f) and Fig. 4. It is clear that the particular value of A_{ex} obtained from a PSSW measurement does have a weak dependency on the adjacent layer, with the addition of the non-magnetic metals (Pt and Ta) giving a greater value of A_{ex}. This is especially evident in the A_{ex} extracted from a consideration of long wavelength spin waves, specifically in the case A_{ex} is determined from all the modes, the PSSW1 mode and the PSSW1 mode of films with t_{NiFe} > 55 nm. This finding reinforces the proposition that the angle between the adjacent spins in the *z*-direction is important in accurately determining the intrinsic value of A_{ex}.

The numerical simulations allowed the PSSW waveform to be investigated. Examples of the waveforms of the simulated OOP spin-wave spectra are presented in Fig. 6. These results demonstrate that the evolution of the PSSW modes is consistent with the expectation that the wavelength of the spin waves decrease with increasing mode number. The displacements of the reduced magnetisation in the x- and y- directions (mx and my respectively) decreases significantly with mode number as expected and in our experiments PSSW3 could not be measured due to its low amplitude. Experimentally, the reduced resonant peak amplitude of the PSSW modes with *p* is shown in Fig. 2. It can be seen that the PSSW1 and PSSW2 resonances possess waveforms consistent with *p*=1 and *p*=2 modes defined in fig.1. These simulations allow the impact of dynamic pinning on the configuration of the spins comprising the resonant modes to be made. Fig. 6 also shows that there is a small deformation of the spin-wave modes in the near-surface region. This confirms that changes to the magnetic state in the interfacial region leads directly to dynamic pinning of PSSW modes.

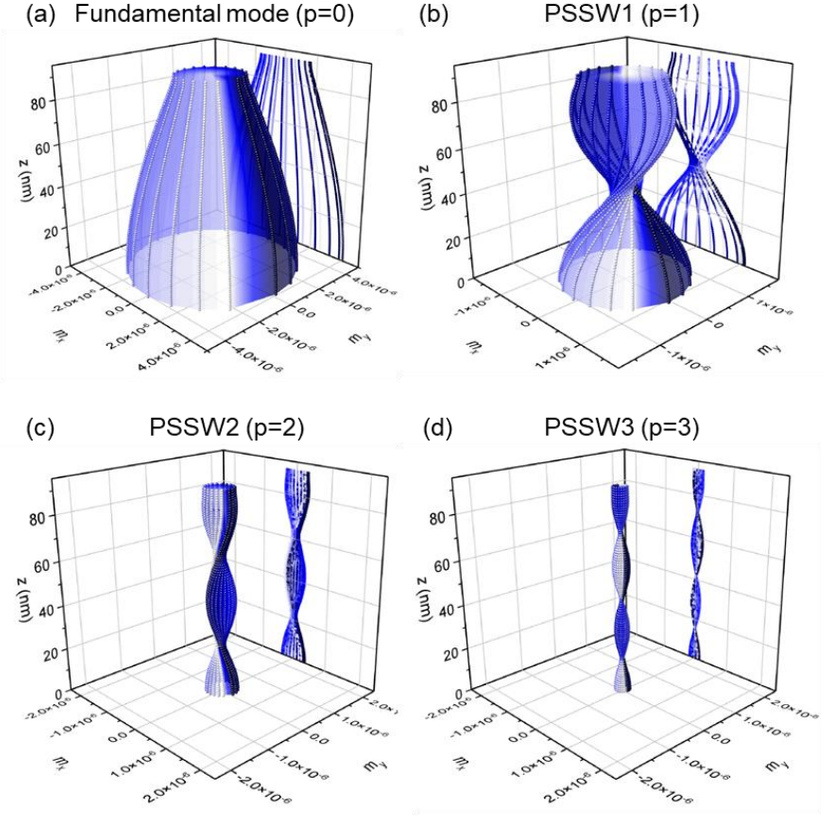

FIG. 6: Simulated example waveforms and projections of spin wave spectra supported by a Ta capped NiFe thin film with NiFe thickness t_{NiFe} = 86 nm. In this simulation, the exchange stiffness constant was set as A_{ex} = 1.3x 10^{-6} erg/cm. a) Fundamental resonance mode (p=0) b) PSSW1 (p=1) c) PSSW2 (p=2) d) PSSW3 (p=3) inset: Zoomed-in figure with same axis labels. The symbols z denotes distance from the substrate and m_x and m_y represents the normalised magnetisation in the x and y directions respectively. The dynamic pinning induced by reduced M_s is set near the top surface (maximum z).

As the dynamic pinning model was first introduced to explain the angle dependence of PSSWs for small rotations of applied magnetic field about the normal, we examined the effect of such rotations on the PSSWs observed. Consistent with the dynamic pinning model, we observe both experimentally and through simulation that the prominence of the PSSW modes reduces significantly with respect to the fundamental mode at angles of $\sim 10^{o}$, appendix B4. This provides additional evidence that the dynamic pinning model is appropriate for these samples. It also suggests that the origin of dynamic pinning is the change in magnetisation in the near-interface region (as modelled) as opposed to forming due to alterations in an anisotropy field that is perpendicular to the film or a different state of strain in the interfacial region [49]. We note that in a previous study of magnetic exchange stiffness in epitaxial $Ni_{1-x}Co_x$(001) films [54], surface anisotropy was found to play a significant role in pinning. Given the different materials involved and the fact that Co and Ni layers in intimate contact are well known to create perpendicular magnetic anisotropy (PMA) these results indicate that pinning mechanisms are material dependent. In the case of NiFe thin films there is scant evident for PMA and even when it is suggested it is clear that its value is small [55]. However, for definitive conclusions on the origin of dynamic pinning, further investigations are required (for additional information regarding the impact of OOP rotation on the PSSWs see Appendix B4).

V. CONCLUSION

In summary, the magnetisation dynamics of a series of NiFe thin films with differing layer thickness and capping layers (uncapped, Pt and Ta) have been explored. The data demonstrates that a simple analysis of PSSWs to extract a single value of the exchange stiffness constant (A_{ex}), based on the rigid pinning model of Kittel (Eq. (1)) is unable to describe the resonant frequencies. This is clearly inconsistent with the normal assumption that the measured exchange stiffness constant is single valued for a given set of thermodynamic variables. In order to address this physical inconsistency, the data are first analysed in terms of an apparent exchange stiffness constant using both the rigid pinning (Kittel) model often found in the literature and a more rigorous generalised wavevector model which allows interface pinning to be parameterised. Numerical modeling has been performed to reconcile the physical expectation of a single exchange stiffness constant with the measured resonances. Attempts to reproduce the experimental data using the rigid pinning model [27] failed and whilst the generalised wavevector model produced consistent values for A_{ex}, the values did not always agree with literature expectations. However, the simulations support a more general pinning condition at the interface, introduced through a dynamic pinning model proposed by Wigen[49], where it was possible to reproduce the measured resonances using a single exchange stiffness constant by modeling the film as a bilayer consisting of a bulk layer with a thin layer of

Journal of Applied Physics
AIP Publishing

reduced magnetisation at the interface between the NiFe and the capping layer. The data also indicates that the material adjacent to the surface influences the value of A_{ex} obtained. Our results suggest that shorter wavelength, higher order PSSWs (eg. PSSW2) are less affected by the changes in dynamic pinning which we hypothesise is due to the larger angle between the spins compromising the PSSWs. Whilst for the range of film thicknesses considered here, we are able to clearly demonstrate a single value of A_{ex} with no indication of any divergence for the thinnest samples. However, it remains an open question as to whether this remains the case for ultra-thin films. These data support the utility of using PSSWs to determine A_{ex}, but show that care must be taken when applying this approach to the complex structures needed for spintronic devices.

ACKNOWLEDGMENTS

The authors gratefully acknowledge the support of the UK EPRSC CDT Graphene NOWNANO through grant number EP/L01548X/1 and the involvement of the facilities of the Henry Royce Institute through EPSRC grants EP/S019367/1 and EP/P025021/1. The authors would like to acknowledge the assistance given by Research IT and the use of the Computational Shared Facility at The University of Manchester. Y.L. acknowledges a scholarship supported by the China Scholarship Council and H.W. acknowledges the support of the EPSRC Doctoral Prize fund through grant number EP/T517823/1.

APPENDIX A: FABRICATION METHODS

1. Thin Film sample preparation

Fabrication of the samples was done using an AJA ATC 2200-V magnetron sputtering system. The substrates employed were Si/SiO_2 where the oxide layer was 290 nm. No deliberate substrate heating was used. The overall structure of the metal layers was $Ni_{0.8}Fe_{0.2}/X$, where X is the capping layer material (either uncapped, Pt capped or Ta capped). The deposition of the Ta, $Ni_{0.8}Fe_{0.2}$ and Pt layers was performed using DC magnetron sputtering from either elemental or, in the case of NiFe, alloy targets. The Ta was deposited at a power of 20 W, with the NiFe and Pt deposited at 100 W. The base pressure prior to deposition was 10^{-8} Torr, with no in situ magnetic fields applied. The working pressure of the Ar^+ gas was 3 mTorr.

APPENDIX B: CHARACTERISATION METHODS

1. Structure Characterization

The structural properties of the layers were determined using X-ray Reflectivity (XRR). The measurements were carried out using a Rigaku Smart Lab system using a 3 kW copper K alpha source. All measurements were performed over a 2θ range of 0.1–8.0 degrees with a step size of 0.01. The data were fitted to a Fresnel model by means of the Parratt recursive algorithm [56] using the GenX simulation package [58]. The fitting was performed until the reduced χ^2 figure of merit was optimized. This provided information on the thickness, roughness and density of the constituent layers. Figure 7 presents the XRR measurement and fit along with the derived structural Scattering Length Density (SLD) for films with t_{NiFe} = 55 nm. Notably, the uncapped and Ta capped cases formed self-terminating oxide layers, as expected. It was found that for the uncapped case the most suitable model to reflect the XRR data was obtained for an oxide layer consisting of a Fe_2O_3/NiO multilayer, which is in agreement with the work of Fitzsimmons et al.[45]. However, it was found that a thinner NiO layer was 0.7 nm which is less than the 1.5 nm reported in [45]. The presence of other iron oxides, such as FeO, in some cases has also reported though in this work a model incorporating a FeO layer could not simulate the XRR data. In the case of Ta capping layer, the Ta oxidized into a self-terminating Ta_2O_5 layer at the

top of the film stack. The roughness of the NiFe/capping layer interface was found to be similar for all samples measured with an average value of 1.7 ± 0.4 nm.

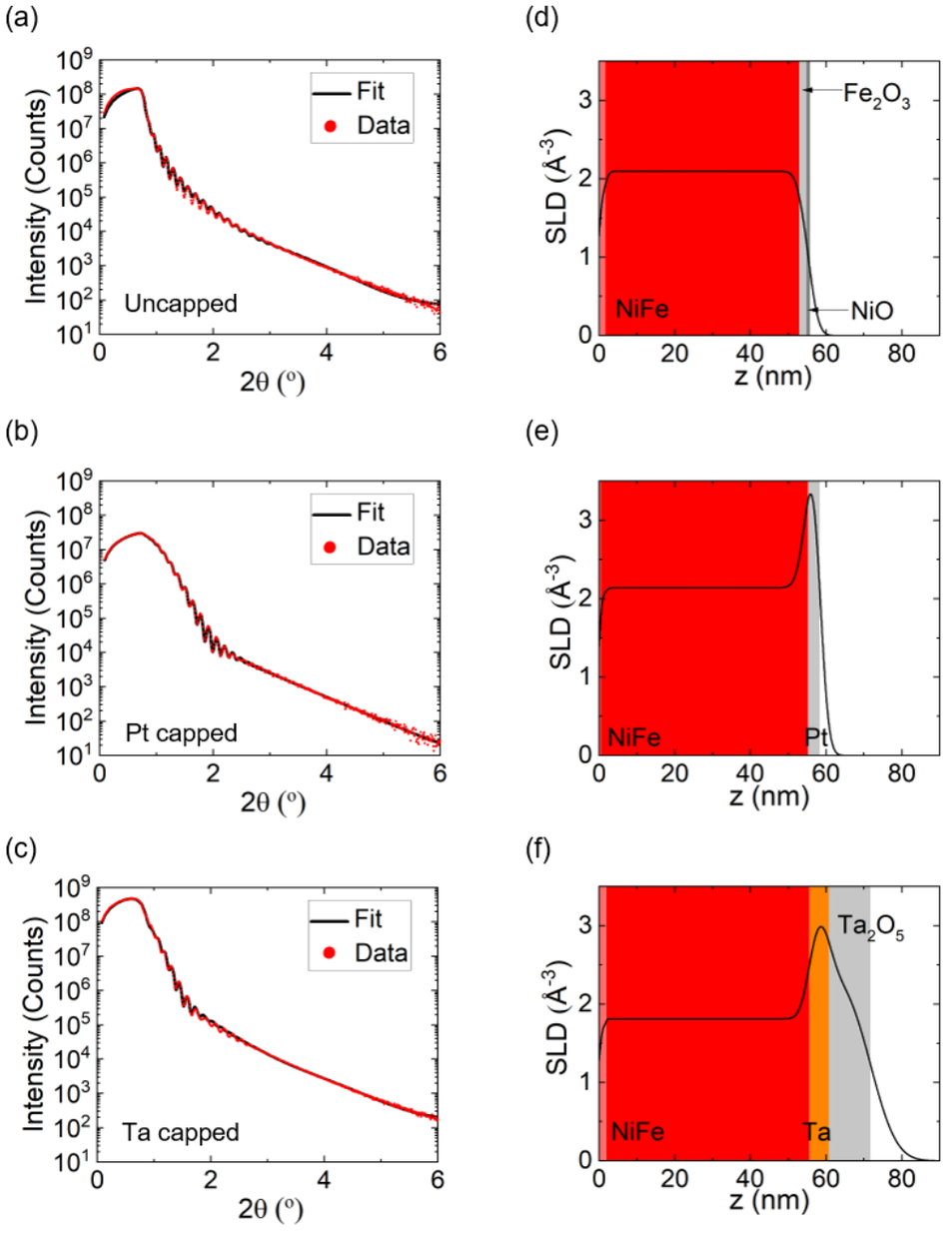

FIG. 7. XRR measurements of the NiFe stacks where NiFe layer thickness is 55 nm for each capping layer case(d-f) Corresponding structural SLDs as derived from the model fits to the XRR measurement as a function of distance from substrate (*z*).

2. Magnetic Measurements

Magnetisation vs applied magnetic field (M-H) loops were measured through Vibrating Sample Magnetometry (VSM) using a Microsense Model 10 vector VSM. The samples were prepared using a Southbay disk cutter to provide an 8-mm disk for the VSM measurement. These measurements were performed using an in-plane applied magnetic field up to 20 kOe to guarantee saturation of the magnetic domain structure. Background correction was applied by obtaining the linear fit to the saturated region of the hysteresis loop, with its

gradient determining the diamagnetic response. The films were found to possess no uniaxial in-plane anisotropy. In Fig. 8, the in-plane and out-of-plane hysteresis loops are shown for the uncapped NiFe film of thickness 86 nm.

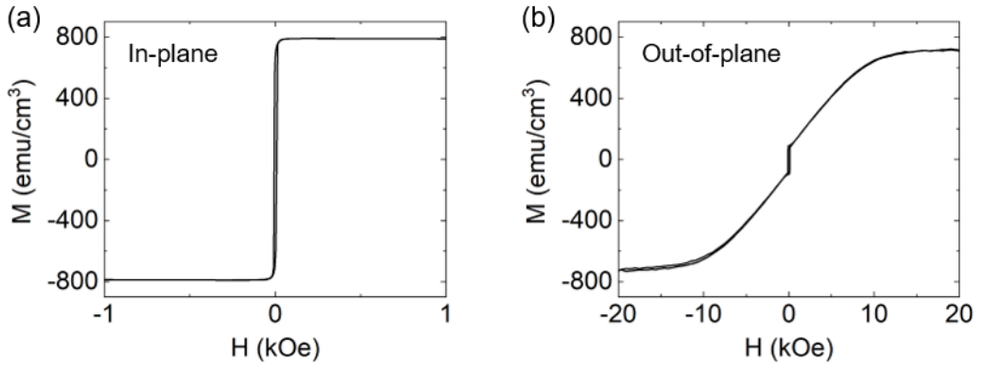

FIG. 8: M-H hysteresis loops for a Ta capped NiFe film with thickness t_{NiFe} = 86 nm at room temperature. The case where the external magnetic field is applied a) in-plane b) out-of-plane.

3. Ferromagnetic resonance measurements

The high frequency properties of the films were determined using a Vector Network Analyzer-Ferromagnetic Resonance (VNA-FMR) setup. This setup employed a picoprobe waveguide and a Keysight VNA N5224A which is capable of frequency measurements in the range 10 MHz to 43.5 GHz. The probes are contacted to a ground-signal-ground waveguide placed in a magnetic field of up to 1.4 T provided by GMW electromagnet. As a flip chip experiment, the sample was placed face-down upon the waveguide, with a natural air barrier sufficient to prevent the shorting of the waveguide. The operating principle of this method is that the magnetic configuration of a film under test will be perturbed by a rf magnetic field due to the current pulses traversing the waveguide. When the frequency of the perturbation by this small magnetic field is equal to the resonant frequency of the system, a large absorption of this rf energy takes place which causes the transmission of energy through the waveguide (measured through the S_{12} parameter) to significantly decrease[26], [48]. The measurements were carried out by performing frequency sweeps for a range of applied external fields as opposed to the conventional field sweeps for set frequencies.

4. Rotational PSSW Measurements

The evolution of the spin-wave spectra as the applied external field was rotated from the OOP direction towards the IP direction was explored up to an angle of 15° and 16° for experiment and simulation respectively. For this investigation, angular increments of 1° (experiment) and 2° (simulation) were selected consistent with previous reports[49], [51]. In the case of simulation, the Pt capped layer possessing an A_{ex} = 1 x10^{-6} erg/cm only was simulated to at an angular increment of 1°. For this investigation the samples possessing t_{NiFe} = 86 nm were studied for each capping layer case, selected due to the greater peak amplitudes provided. This was particularly important to ensure detection of the PSSWs due to the lower sensitivity of the NanOsc. Waveguide employed in this study as opposed to the PicoProbe waveguide used in the other dynamic measurements (see Appendix B3).

In Fig. 9 (a-b), the variation of the ratio of the peak amplitude of PSSW1 to the peak amplitude of the FMR mode is shown as a function of angle where 0° is the out-of-plane direction for both the measurements and simulations. Two observations can be made. Firstly, the peak amplitude of the PSSW1 peak reduces by a

similar relative amount in both the experiments and simulation which is consistent with theory for dynamic pinning. Secondly, the amplitude ratios are different between the experimental results and the simulation by approximately a factor of 10. This is not unexpected as neither our experiment nor model are calibrated. A comparison of the simulated resonant frequencies of the NiFe films in all capping layer cases with the experimental data is shown in Fig. 9 (c-e). The results of the numerical simulations and the experimental findings are in agreement, with similar increases in resonant frequencies with in-plane rotation exhibited. As expected, it is seen that a higher A_{ex} results in a greater increase of the frequencies of the modes [51].

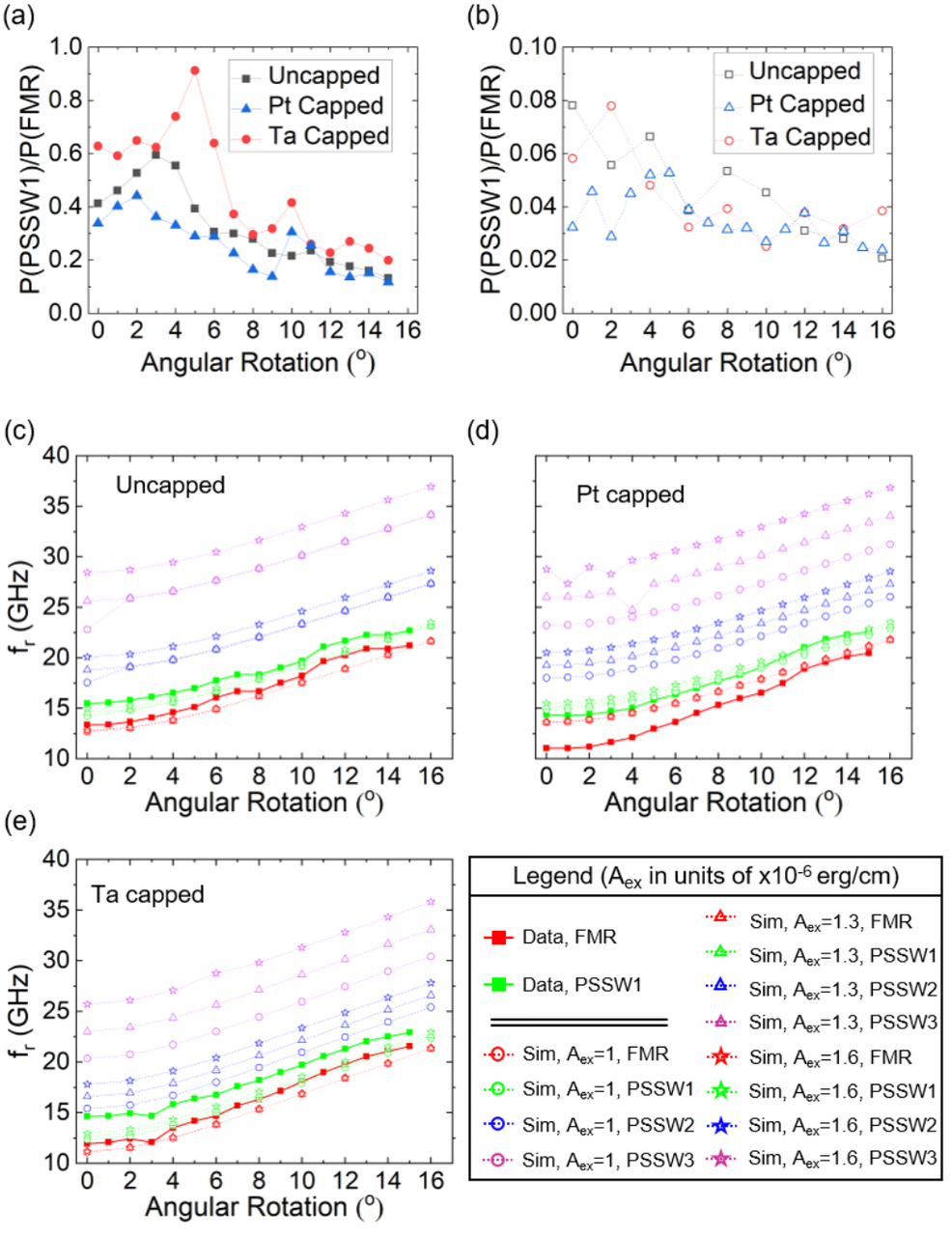

FIG. 9: Experimentally measured and numerically modelled evolution of spin wave spectra with out-of-plane angular rotation of the external field. (a-b) The ratio of the peak amplitude of PSSW1 to that of the FMR mode, as the external field is rotation from the out-of-plane direction. These data are for an 86nm thick NiFe film. a)

Experimental measurements b) Simulation results. The y-axis label P(PSSW1) and P(FMR) refer to the peak amplitude of the PSSW1 and FMR mode respectively. (c-e) Measured and simulated resonant frequencies of the spin-wave spectra exhibited by the films with NiFe thicknesses 86 nm with rotation of the external field from the out-of-plane direction in the following capping layer cases a) Uncapped b) Pt capped c) Ta capped. A range of exchange stiffness constants are explored in the simulation.

Appendix C: Simulation Methods

Based on the micromagnetic model, resonant dynamics of magnetization is characterised by solving the Landau-Lifshitz equation (C1) [57]

$$\frac{\partial \mathbf{m}}{\partial t} = \frac{\gamma}{1+\alpha^2}\{\mathbf{m} \times \mathbf{H}_{\text{eff}} + \alpha[\mathbf{m} \times (\mathbf{m} \times \mathbf{H}_{\text{eff}})]\}, \quad \text{(C1)}$$

where **m** indicates the normalised magnetization in constant magnitude M_s = **M**/**m**, with the damping parameter α and the gyromagnetic ratio of the electron γ. The effective field $\mathbf{H}_{\text{eff}}$ applied on the magnetization is defined as $\mathbf{H}_{\text{eff}} = -\mu_0^{-1}\delta E/\delta \mathbf{M}$, which is based on the total energy E that comprises of the symmetric exchange interaction, the Zeeman coupling and the magnetostatic interaction. In order to guarantee the accuracy of the dynamic simulations, the Landau-Lifshitz equation is solved by Runge–Kutta method (RK45) with a maximum timestep 10^{-6} ns. In the dynamic simulations we use the damping parameter α = 0.001. Note that much smaller timesteps and different damping parameter in the underdamped range ($0 < \alpha < 1$) have been tested and similar results obtained.

Our simulations are implemented by the finite-difference GPU-accelerated micromagnetic program, mumax³[50]. Unless specified otherwise, the sample is described by a bilayer structure with $FM_1(t_{NiFe})$/$FM_2(t_{red})$ where t_{NiFe} is the NiFe layer thickness and t_{red} is the reduced magnetisation layer thickness. In order to minimize the demagnetization effects from the geometric edges, the dimension in the *xy*-plane is set to 128 nm × 128 nm with periodic boundary conditions applied in the plane, and the overall system is discretized into 2 nm × 2 nm × 1 nm cuboid cells. In the ringdown method [58] the system is initialized to a field-polarized state, followed by a weak magnetic excitation h_{exc} applied for 20 ns to perturb it from its equilibrium, and the magnetization dynamics are sampled and recorded with a 10^{-4} ns timestep, where at least 100 steps are solved between the recorded data points. Subsequently, a fast Fourier Transform (FFT) is used to obtain the amplitude spectrum of the averaged magnetization, and the characterized frequency is extracted from the measured time-domain. Rigid pinning put forth by Kittel was modelled using frozen spins at the interface. In the uncapped case, due to the antiferromagnetic nature of the self-terminating Fe_2O_3/NiO bilayer formed due to oxidization of the NiFe surface, the approach of modeling antiferromagnets with mumax³ outlined by De Clercq [53] was utilized. The waveform of the Perpendicular Standing Spin Waves (PSSWs) was extracted from an assessment of the depth-resolved m_x and m_y magnetization vectors when the structure is excited at a frequency equal to the resonant frequency of each resonant mode.

References

[1] T. Thomson, "Magnetic properties of metallic thin films," in *Metallic Films for Electronic, Optical and Magnetic Applications: Structure, Processing and Properties*, 2013, pp. 454–546. doi: 10.1533/9780857096296.2.454.

[2] A. V. Chumak, V. I. Vasyuchka, A. A. Serga, and B. Hillebrands, "Magnon spintronics," *Nat Phys*, vol. 11, no. 6, pp. 453–461, 2015, doi: 10.1038/nphys3347.

[3] J. Walowski and M. Münzenberg, "Perspective: Ultrafast magnetism and THz spintronics," *J Appl Phys*, vol. 120, no. 14, p. 140901, 2016, doi: 10.1063/1.4958846.

[4] A. Barman and A. Haldar, "Time-Domain study of magnetization dynamics in magnetic thin films and micro- and nanostructures," *Solid State Physics*, vol. 65, pp. 1–108, 2014, doi: 10.1016/B978-0-12-800175-2.00001-7.

[5] R. L. Stamps *et al.*, "The 2014 Magnetism Roadmap," *J Phys D Appl Phys*, vol. 47, no. 33, p. 333001, 2014, doi: 10.1088/0022-3727/47/33/333001.

[6] B. Dieny *et al.*, "Opportunities and challenges for spintronics in the microelectronics industry," *Nat Electron*, vol. 3, no. 8, pp. 446–459, 2020, doi: 10.1038/s41928-020-0461-5.

[7] E. E. Fullerton and J. R. Childress, "Spintronics, Magnetoresistive Heads, and the Emergence of the Digital World," *Proceedings of the IEEE*, vol. 104, no. 10, pp. 1787–1795, 2016, doi: 10.1109/JPROC.2016.2567778.

[8] S. Parkin, X. Jiang, C. Kaiser, A. Panchula, K. Roche, and M. Samant, "Magnetically engineered spintronic sensors and memory," *Proceedings of the IEEE*, vol. 91, no. 5, pp. 661–679, 2003, doi: 10.1109/JPROC.2003.811807.

[9] A. Hirohata *et al.*, "Review on spintronics: Principles and device applications," *J Magn Magn Mater*, vol. 509, p. 166711, 2020, doi: 10.1016/j.jmmm.2020.166711.

[10] T. Chen *et al.*, "Spin-Torque and Spin-Hall Nano-Oscillators," *Proceedings of the IEEE*, vol. 104, no. 10, pp. 1919–1945, 2016, doi: 10.1109/JPROC.2016.2554518.

[11] V. G. Harris, "Modern microwave ferrites," *IEEE Trans Magn*, vol. 48, no. 3, pp. 1075–1104, 2012, doi: 10.1109/TMAG.2011.2180732.

[12] P. P. Freitas, R. Ferreira, and S. Cardoso, "Spintronic Sensors," *Proceedings of the IEEE*, vol. 104, no. 10, pp. 1894–1918, 2016, doi: 10.1109/JPROC.2016.2578303.

[13] D. B. Gopman, J. W. Lau, K. P. Mohanchandra, K. Wetzlar, and G. P. Carman, "Determination of the exchange constant of Tb_{0.3}Dy0.7Fe2 by broadband ferromagnetic resonance spectroscopy," *Phys Rev B*, vol. 93, no. 6, p. 064425, 2016, doi: 10.1103/PhysRevB.93.064425.

[14] J. Leliaert and J. Mulkers, "Tomorrow's micromagnetic simulations," *J Appl Phys*, vol. 125, no. 18, p. 180901, 2019, doi: 10.1063/1.5093730.

[15] J. M. D. Coey, *Magnetism and Magnetic Materials*. 2010.

[16] H. Nosé, "Exchange integral in Ni and its alloy film from spin wave resonance," *J Physical Soc Japan*, vol. 16, no. 12, pp. 2475–2481, 1961.

[17] S. Klingler *et al.*, "Measurements of the exchange stiffness of YIG films using broadband ferromagnetic resonance techniques," *J Phys D Appl Phys*, vol. 48, no. 1, p. 015001, 2014, doi: 10.1088/0022-3727/48/1/015001.

[18] Y. Yin *et al.*, "Tunable permalloy-based films for magnonic devices," *Phys Rev B*, vol. 92, no. 2, p. 24427, Jul. 2015, doi: 10.1103/PhysRevB.92.024427.

[19] X. Liu, M. M. Steiner, R. Sooryakumar, G. Prinz, R. F. C. Farrow, and G. Harp, "Exchange stiffness, magnetization, and spin waves in cubic and hexagonal phases of cobalt," *Phys Rev B*, vol. 53, no. 18, p. 12166, 1996.

[20] B. Hillebrands and J. Hamrle, "Investigation of spin waves and spin dynamics by optical techniques," in *Handbook of Magnetism and Advanced Magnetic Materials*, Wiley, 2007.

[21] S. P. Vernon, S. M. Lindsay, and M. B. Stearns, "Brillouin scattering from thermal magnons in a thin Co film," *Phys Rev B*, vol. 29, no. 8, pp. 4439–4442, 1984, doi: 10.1103/PhysRevB.29.4439.

[22] G. A. Riley, J. M. Shaw, T. J. Silva, and H. T. Nembach, "Simultaneous measurement of the exchange parameter and saturation magnetization using propagating spin waves," *Appl Phys Lett*, vol. 120, no. 11, p. 112405, 2022, doi: 10.1063/5.0083583.

[23] S. O. Demokritov, B. Hillebrands, and A. N. Slavin, "Brillouin light scattering studies of confined spin waves: Linear and nonlinear confinement," *Physics Report*, vol. 348, no. 6, pp. 441–489, 2001, doi: 10.1016/S0370-1573(00)00116-2.

[24] S. O. Demokritov and V. E. Demidov, "Micro-brillouin light scattering spectroscopy of magnetic nanostructures," *IEEE Trans Magn*, vol. 44, no. 1, pp. 6–12, 2007, doi: 10.1109/TMAG.2007.910227.

[25] J. P. Bick *et al.*, "Exchange-stiffness constant of a Nd-Fe-B based nanocomposite determined by magnetic neutron scattering," *Appl Phys Lett*, vol. 103, no. 12, p. 122402, 2013, doi: 10.1063/1.4821453.

[26] I. S. Maksymov and M. Kostylev, "Broadband stripline ferromagnetic resonance spectroscopy of ferromagnetic films, multilayers and nanostructures," *Physica E Low Dimens Syst Nanostruct*, vol. 69, no. August, pp. 253–293, 2015, doi: 10.1016/j.physe.2014.12.027.

[27] C. Kittel, "Excitation of Spin Waves in a Ferromagnet by a Uniform rf Field," *Physical Review*, vol. 110, no. 5, pp. 1295–1297, 1958.

[28] M. H. Seavey and P. E. Tannenwald, "Direct Observation of Spin-Wave Resonance," *Phys Rev Lett*, vol. 1, no. 5, pp. 168–169, Sep. 1958, doi: 10.1103/PhysRevLett.1.168.

[29] A. G. Gurevich and G. A. Melkov, *Magnetisation Oscillations and Waves*. CRC Press, 1996.

[30] W. S. Ament and G. T. Rado, "Electromagnetic effects of spin wave resonance in ferromagnetic metals," *Physical Review*, vol. 97, no. 6, pp. 1558–1566, 1955, doi: 10.1103/PhysRev.97.1558.

[31] G. T. Rado and J. R. Weertman, "Spin-wave resonance in a ferromagnetic metal," *Journal of Physics and Chemistry of Solids*, vol. 11, no. 3–4, pp. 315–333, 1959, doi: 10.1016/0022-3697(59)90233-1.

[32] C. F. Kooi, P. E. Wigen, M. R. Shanabarger, and J. V. Kerrigan, "Spin-Wave Resonance in Magnetic Films on the Basis of the Surface-Spin-Pinning Model and the Volume Inhomogeneity Model," *J Appl Phys*, vol. 35, no. 3, pp. 791–797, 1964.

[33] B. Samantaray, A. K. Singh, C. Banerjee, A. Barman, A. Perumal, and P. Mandal, "Perpendicular standing spin wave and magnetic anisotropic study on amorphous FeTaC films," *IEEE Trans Magn*, vol. 52, no. 7, pp. 1–4, 2016, doi: 10.1109/TMAG.2016.2520981.

[34] J. BenYoussef *et al.*, "Ferromagnetic resonance in epitaxial FePd thin films with perpendicular anisotropy," *J Magn Magn Mater*, vol. 202, no. 2, pp. 277–284, 1999, doi: 10.1016/S0304-8853(99)00413-8.

[35] T. D. Rossing, "Spin-Wave Resonance in Thin Films at Oblique Angles," *J Appl Phys*, vol. 34, no. 4, pp. 1133--1135, 1963.

[36] C. Bilzer *et al.*, "Study of the dynamic magnetic properties of soft CoFeB films," *J Appl Phys*, vol. 100, no. 5, p. 053903, 2006, doi: 10.1063/1.2337165.

[37] A. Conca *et al.*, "Annealing influence on the Gilbert damping parameter and the exchange constant of CoFeB thin films," *Appl Phys Lett*, vol. 104, no. 18, p. 182407, 2014, doi: 10.1063/1.4875927.

[38] M. Belmeguenai *et al.*, "Microstrip line ferromagnetic resonance and Brillouin light scattering investigations of magnetic properties of Co 2 MnGe Heusler thin films," *Phys Rev B*, vol. 79, no. 2, p. 024419, 2009, doi: 10.1103/PhysRevB.79.024419.

[39] H. Puszkarski, "Theory of Surface-states in Spin-wave Resonance," *Prog Surf Sci*, vol. 9, no. 5–6, pp. 191–247, 1979, doi: 10.1016/0079-6816(79)90013-3.

[40] A. Maksymowicz, "Spin-wave spectra of insulating films: Comparison of exact calculations and a single-wave-vector model," *Phys Rev B*, vol. 33, no. 9, pp. 6045–6053, May 1986, doi: 10.1103/PhysRevB.33.6045.

[41] A. Fert, "Origin, development, and future of spintronics (nobel lecture)," *Angewandte Chemie International Edition*, vol. 47, no. 32, pp. 5956–5967, 2008, doi: 10.1002/anie.200801093.

[42] S. A. Wolf, A. Y. Chtchelkanova, and D. M. Treger, "Spintronics - A retrospective and perspective," *IBM J Res Dev*, vol. 50, no. 1, pp. 101–110, 2006, doi: 10.1147/rd.501.0101.

[43] W. Kwiatkowski and S. Tumanski, "The permalloy magnetoresistive sensors-properties and applications," *J Phys E*, vol. 19, no. 7, p. 502, 1986.

[44] A. T. English and G. Y. Chin, "Metallurgy and magnetic properties control in permalloy," *J Appl Phys*, vol. 38, no. 3, pp. 1183--1187, 1967.

[45] M. R. Fitzsimmons, T. J. Silva, and T. M. Crawford, "Surface Oxidation of Permalloy Thin Films," *Phys Rev B*, vol. 73, no. 1, p. 014420, 2006.

[46] G. Nahrwold, J. M. Scholtyssek, S. Motl-Ziegler, O. Albrecht, U. Merkt, and G. Meier, "Structural, magnetic, and transport properties of Permalloy for spintronic experiments," *J Appl Phys*, vol. 108, no. 1, p. 013907, 2010.

[47] M. Björck and G. Andersson, "GenX: An extensible X-ray reflectivity refinement program utilizing differential evolution," *J Appl Crystallogr*, vol. 40, no. 6, pp. 1174–1178, 2007, doi: 10.1107/S0021889807045086.

[48] C. Kittel, "On the theory of ferromagnetic resonance absorption," *Physical Review*, vol. 73, no. 2, pp. 155–161, 1948, doi: 10.1103/PhysRev.73.155.

[49] P. E. Wigen, C. F. Kooi, M. R. Shanabarger, and T. D. Rossing, "Dynamic pinning in thin-film spin-wave resonance," *Phys Rev Lett*, vol. 9, no. 5, pp. 206–208, 1962, doi: 10.1103/PhysRevLett.9.206.

[50] A. Vansteenkiste, J. Leliaert, M. Dvornik, M. Helsen, F. Garcia-Sanchez, and B. Van Waeyenberge, "The design and verification of MuMax3," *AIP Adv*, vol. 4, no. 10, 2014, doi: 10.1063/1.4899186.

[51] P. E. Wigen, C. F. Kooi, M. R. Shanabarger, U. K. Cummings, and M. E. Baldwin, "Angular dependence of spin pinning in thin ferromagnetic films," *J Appl Phys*, vol. 34, no. 4, pp. 1137–1139, 1963, doi: 10.1063/1.1729405.

[52] R. F. L. Evans, W. J. Fan, P. Chureemart, T. A. Ostler, M. O. A. Ellis, and R. W. Chantrell, "Atomistic spin model simulations of magnetic nanomaterials," *Journal of Physics: Condensed Matter*, vol. 26, no. 10, p. 103202, Mar. 2014, doi: 10.1088/0953-8984/26/10/103202.

[53] J. De Clercq, J. Leliaert, and B. Van Waeyenberge, "Modelling compensated antiferromagnetic interfaces with mumax^3," *J Phys D Appl Phys*, vol. 50, no. 42, p. 425002, 2017.

[54] P. Talagala *et al.*, "Determination of magnetic exchange stiffness and surface anisotropy constants in epitaxial (formula presented) films," *Phys Rev B Condens Matter Mater Phys*, vol. 66, no. 14, 2002, doi: 10.1103/PhysRevB.66.144426.

[55] S. Hirayama, S. Kasai, and S. Mitani, "Interface perpendicular magnetic anisotropy in ultrathin Ta/NiFe/Pt layered structures," *Jpn J Appl Phys*, vol. 57, no. 1, 2018, doi: 10.7567/JJAP.57.013001.

[56] L. G. Parratt, "Surface Studies of Solids," *Physical Review*, vol. 95, no. 2, p. 359, 1954.

[57] L. D. Landau and E. M. Lifshitz, "Theory of the Dispersion of Magnetic Permeability in Ferromagnetic Bodies," *Phys. Z. Sowietunion*, vol. 8, p. 153, 1935, doi: 10.1016/b978-0-08-010523-9.50018-3.

[58] A. Baker *et al.*, "Proposal of a micromagnetic standard problem for ferromagnetic resonance simulations," *J Magn Magn Mater*, vol. 421, pp. 428–439, 2017, doi: 10.1016/j.jmmm.2016.08.009.

AIP Publishing

Journal of Applied Physics

ACCEPTED MANUSCRIPT

PLEASE CITE THIS ARTICLE AS DOI: 10.1063/5.0135024

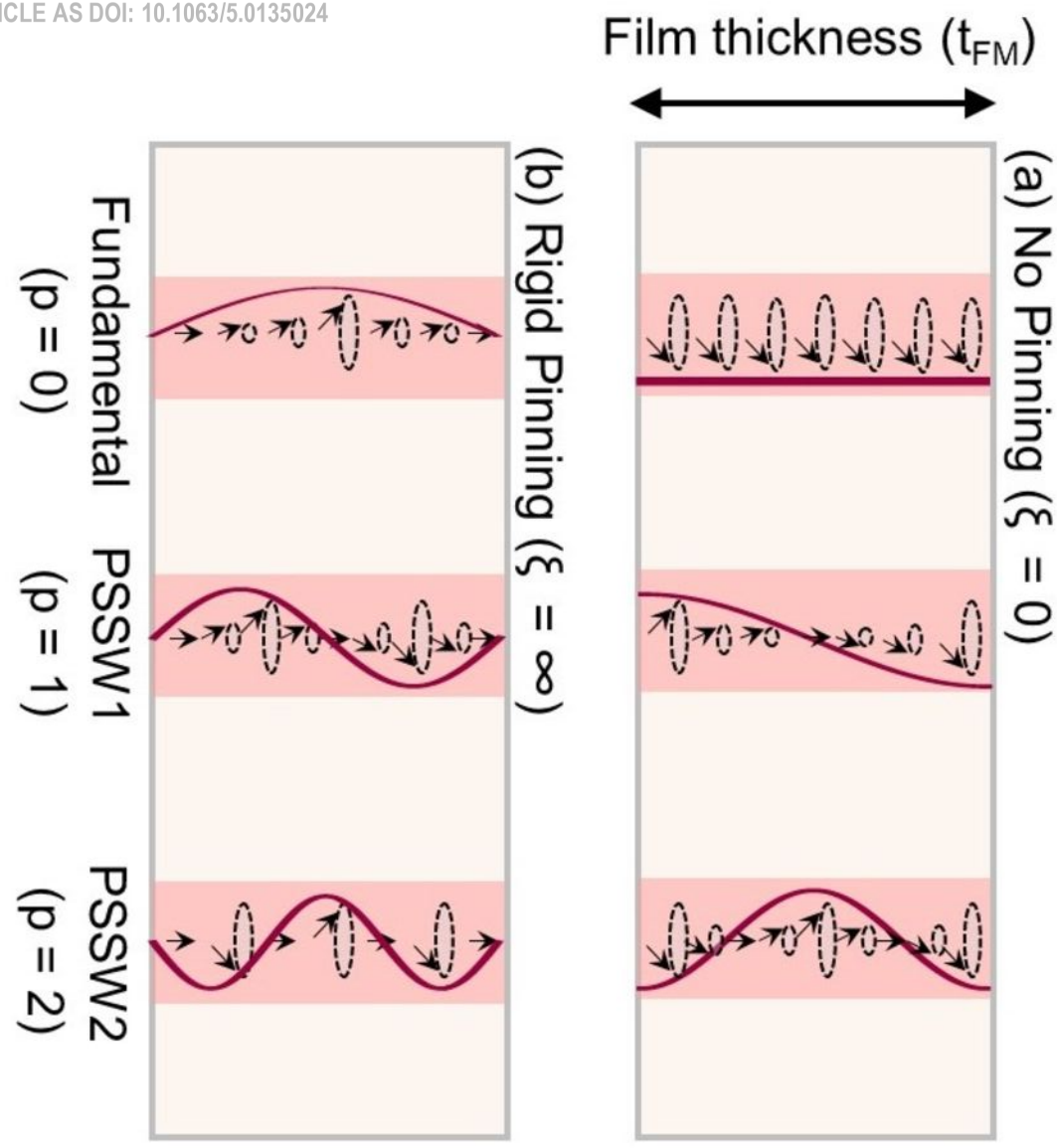

AIP Publishing

Journal of Applied Physics

PLEASE CITE THIS ARTICLE AS DOI: 10.1063/5.0135024

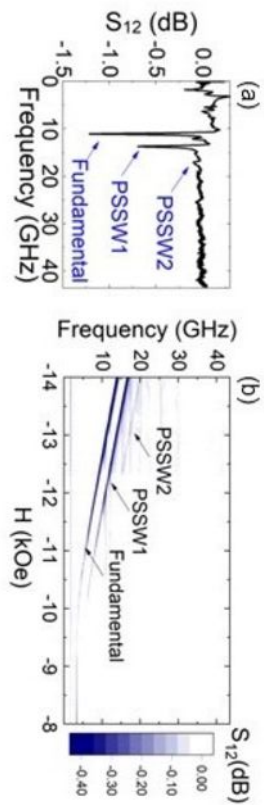

Journal of Applied Physics

AIP Publishing

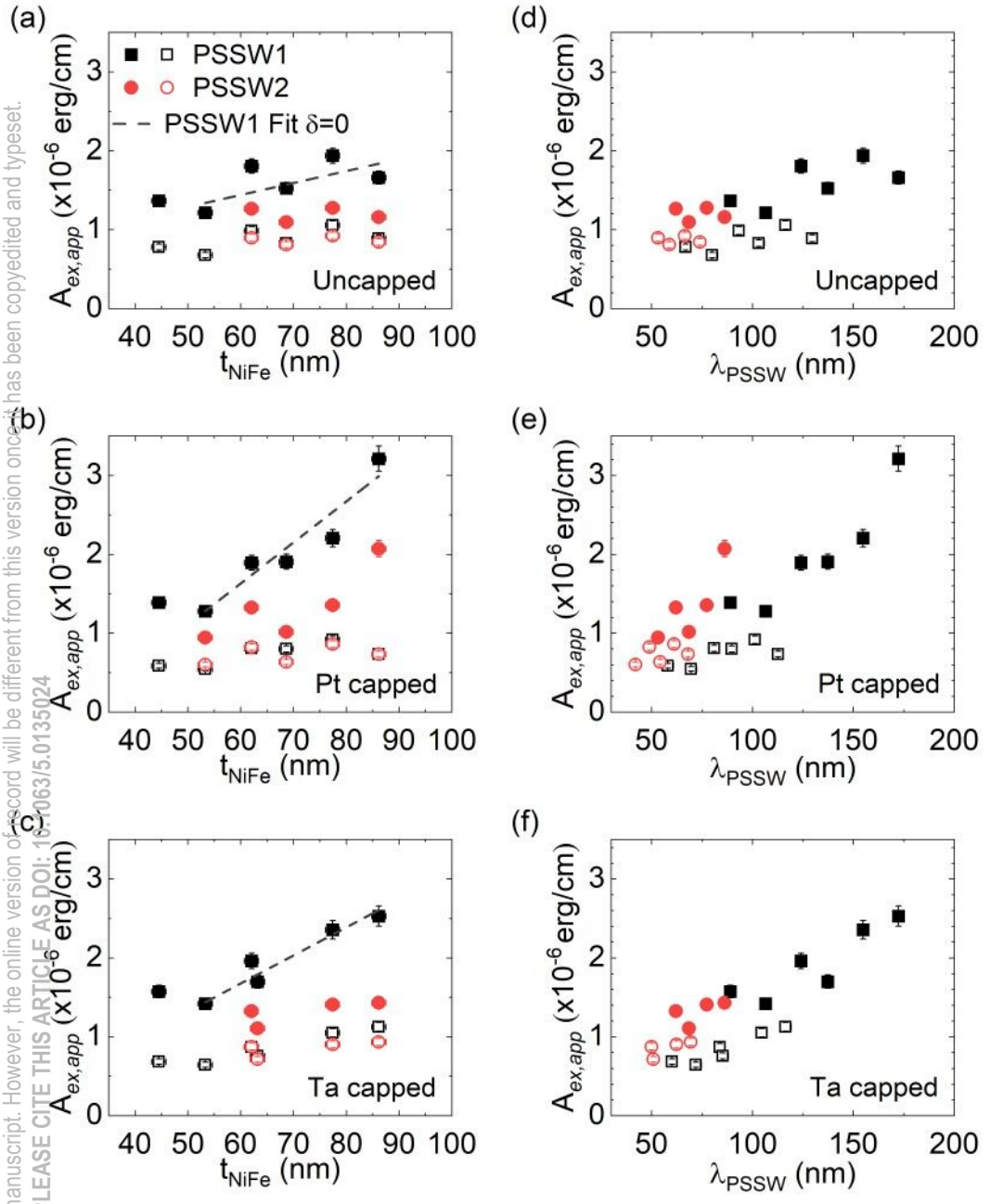

AIP Publishing

Journal of Applied Physics

ACCEPTED MANUSCRIPT

PLEASE CITE THIS ARTICLE AS DOI: 10.1063/5.0135024

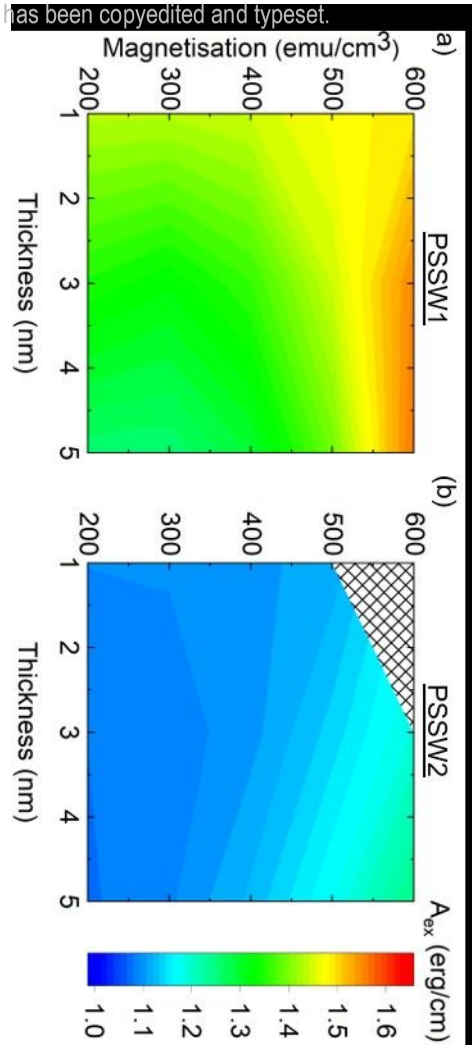

Journal of Applied Physics

AIP Publishing

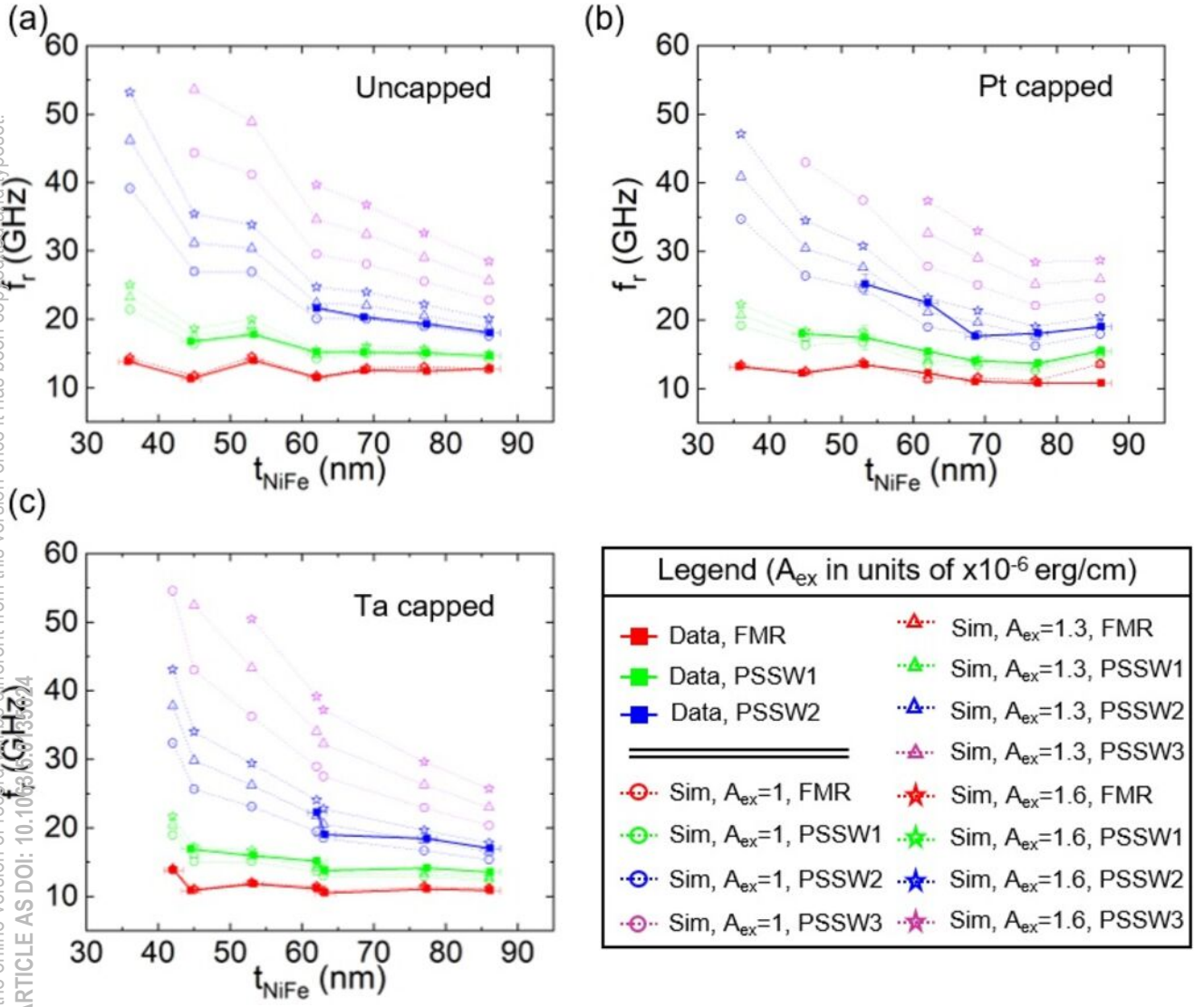

AIP Publishing

Journal of Applied Physics

ACCEPTED MANUSCRIPT

PLEASE CITE THIS ARTICLE AS DOI: 10.1063/5.0135024

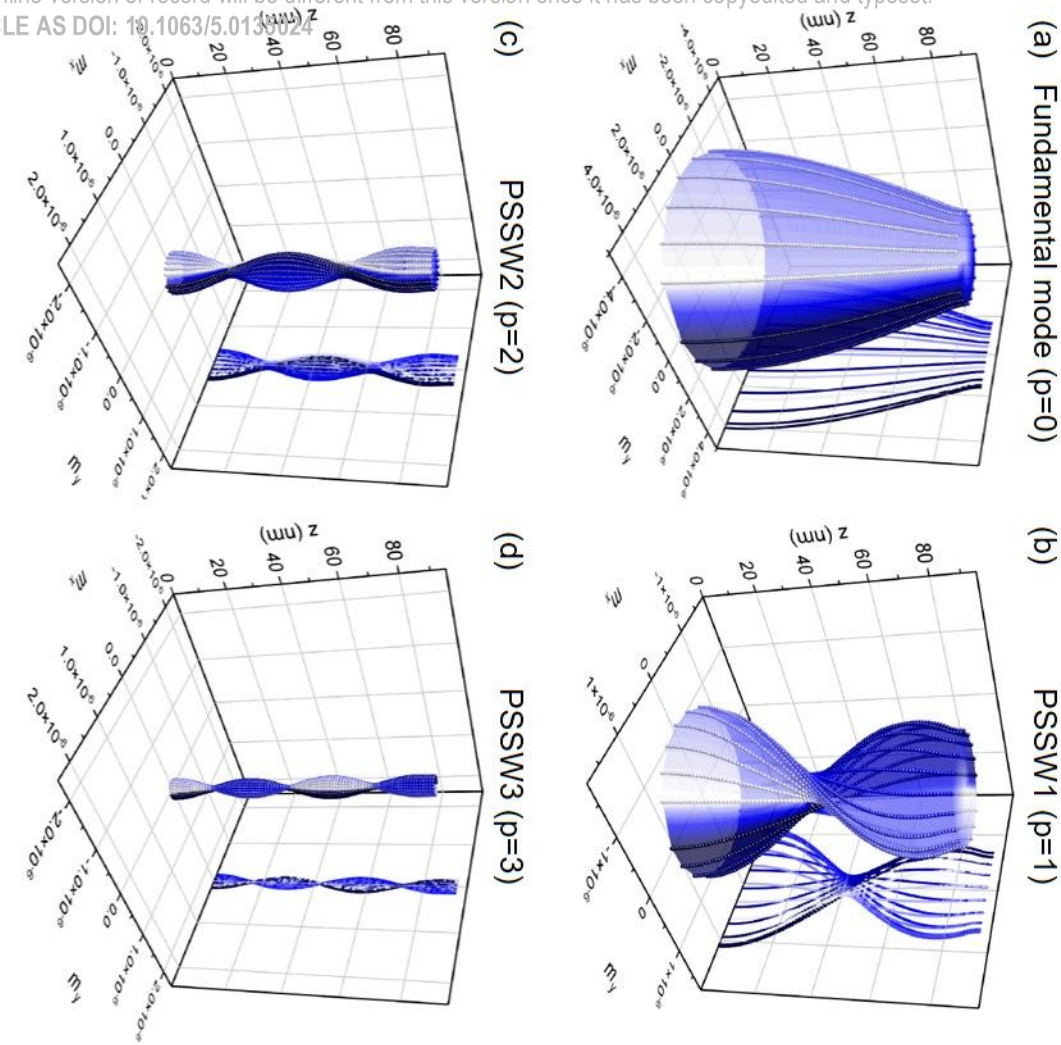

AIP Publishing

Journal of Applied Physics

PLEASE CITE THIS ARTICLE AS DOI: 10.1063/5.0135024

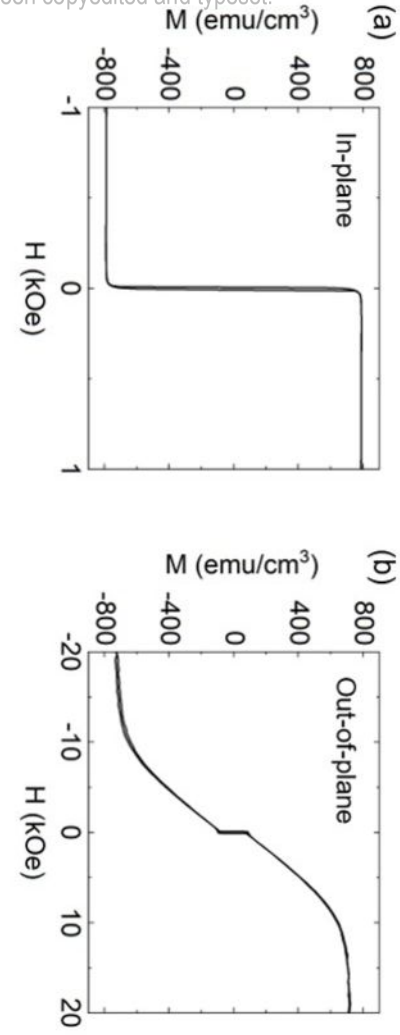

Journal of Applied Physics

AIP Publishing